



Wigner analysis of electron correlation in high-order above-threshold ionizationMengWen Shi ^{1,2} XuanYang Lai ^{1,*} ShaoGang Yu,¹ YanLan Wang,¹ Wei Quan,¹ and XiaoJun Liu^{1,†}¹*State Key Laboratory of Magnetic Resonance and Atomic and Molecular Physics, Wuhan Institute of Physics and Mathematics, Innovation Academy for Precision Measurement Science and Technology, Chinese Academy of Sciences, Wuhan 430071, China*²*School of Physical Sciences, University of Chinese Academy of Sciences, Beijing 100049, China*

(Received 24 September 2021; accepted 13 January 2022; published 28 January 2022)

We theoretically investigate the electron correlation effect on high-order above-threshold ionization (HATI) of the helium atom, by numerically solving the time-dependent Schrödinger equation. Our simulations show that, due to the electron correlation effect, the HATI amplitude shows a significant enhancement, and moreover, such an enhancement becomes weak for the long laser wavelength or high laser intensity. In terms of a Wigner analysis, we reveal that the HATI enhancement is caused by the Coulomb exclusion between the two electrons during the rescattering. With the increase of laser wavelength or intensity, the return energy of the rescattered electron increases, and accordingly, the Coulomb exclusion effect decreases relatively, leading to that the HATI enhancement becomes weak. Our work provides a deep insight into the two-electron correlated dynamics during the strong-field ionization.

DOI: [10.1103/PhysRevA.105.013118](https://doi.org/10.1103/PhysRevA.105.013118)**I. INTRODUCTION**

When an atom or a molecule interacts with an intense laser field, the outmost bound electron may be ionized by absorbing more photons than necessary. This phenomenon is called above-threshold ionization (ATI) and has attracted increasing attention since its first discovery [1]. The corresponding photoelectron energy spectrum shows a series of peaks separated by the energy of one photon. In addition, in the high-energy part of the spectrum, there is a peculiar plateau structure followed by a cutoff [2,3]. This feature is named as high-order ATI (HATI) and the physical mechanism behind this phenomenon can be understood with a three-step model [4,5]: the bound electron in an atom is (i) first released into the continuum, (ii) subsequently accelerated by the laser field, and (iii) may return to the core and elastically scatters off the core to obtain more energy from the laser field. Recently, significant progress has been made in the study of (H)ATI. For example, the ATI has been used to retrieve the structure and dynamics of the valence-electron cloud in atoms on a sub-10-as timescale [6], to observe the symmetry of the highest-occupied molecular orbital (HOMO) of N₂ and O₂ [7], and to calibrate the carrier-envelope phase of the few-cycle laser field [8,9]. On the other side, based on the rescattering process behind the HATI, a so-called laser-induced electron diffraction (LIED) scheme was successfully employed in probing the molecular structure and ultrafast dynamics [7,10–12].

Usually, the understanding and the application of ATI is based on single active electron (SAE) approximation. Until recently, the fingerprint of the multi-electron effect on the

ATI was revealed [13–20]. For example, after the atom is ionized, the remaining bound electrons can be also driven by the laser field, leading to the generation of a dynamic core polarization [16–18]. It has been shown that, after considering the dynamic core polarization, the calculated ionization yields of CO versus the orientation angle agree better with the data than that simulated within SAE [16]. On the other hand, it has been found that the multi-electron effect also affects the back-rescattered electron. For example, the solution of the time-dependent Schrödinger equation (TDSE) showed that the HATI amplitude of an atom with two active electrons (TAE) is much larger than that computed within the SAE, and moreover, this difference decreases with the increase of laser wavelength [20]. However, how the electron correlation leads to the enhancement of the HATI amplitude and why the HATI enhancement becomes negligible in the long-wavelength regime have not yet been discussed. The main reason for this is that the sole TDSE solution cannot give a clear physical picture for the electron-correlation dynamics during the strong-field ionization.

In this work, we theoretically study the electron correlation effect on the HATI by numerically solving the TDSE of a He atom with TAE. We find that the HATI amplitude shows a significant enhancement in comparison with the result computed with SAE, and moreover, the HATI enhancement becomes weak with the increase of laser wavelength or laser intensity. In terms of a Wigner analysis, which provides a reexpression of quantum mechanics based on classical concepts in a phase space, we reveal that the HATI enhancement is mainly caused by the Coulomb exclusion between the two electrons during the rescattering. With the increase of laser wavelength or laser intensity, the return energy of the rescattered electron increases. Accordingly, the Coulomb exclusion effect between the two electrons becomes relatively weak, leading to a less significant HATI enhancement.

*xylai@wipm.ac.cn

†xjliu@wipm.ac.cn

This paper is organized as follows. In Sec. II, we briefly recall the numerical solution of TDSE and the Wigner distributions. Subsequently, we present and compare the photoelectron momentum distribution with TAE and SAE. By using the Wigner distributions, the underlying physics of the electron correlation effects in the HATI is revealed. Finally, our conclusions are given in Sec. IV. Atomic units (a.u.) are used throughout this paper unless otherwise stated.

II. THEORETICAL METHODS

A. Time-dependent Schrödinger equation

In this work, the ionization of He in a strong laser field is simulated by numerically solving TDSE in one dimension [21–23]:

$$i\frac{\partial}{\partial t}\Psi(x_1, x_2, t) = H\Psi(x_1, x_2, t). \quad (1)$$

The total Hamiltonian in the length gauge and dipole approximation is given by

$$H = \frac{p_1^2}{2} + \frac{p_2^2}{2} + V(x_1) + V(x_2) + U(x_1, x_2) + (x_1 + x_2)E(t), \quad (2)$$

where $V(x) = -\frac{2}{\sqrt{x^2+a}}$ and $U(x_1, x_2) = \frac{1}{\sqrt{(x_1-x_2)^2+b}}$ with the softening parameters a and b . In practice, the ground state of He is obtained with the imaginary-time propagation method [24] and then is evolved with a split-operator method [25,26]. By projecting the final state $\Psi(x_1, x_2, \infty)$ onto the different bound states of He^+ , the correlated wave packet of the first electron can be obtained

$$\psi_j(x_1) = \langle \varphi_j(x_2) | \Psi(x_1, x_2, \infty) \rangle, \quad (3)$$

where ψ and φ are the wave packets of the first electron and He^+ core, respectively, and the index j denotes the j th eigenstate of He^+ . The portion of the wave packet ψ_j far away from the core is considered to be ionized and is used to obtain the photoelectron momentum distribution (PMD), $|C_j(p_1)|^2$, by using a Fourier transform method [27]. The total PMD is written as a superposition of all PMDs related to different ionic states of He^+ , i.e., $M(p_1) = \sum_j |C_j(p_1)|^2$.

In our simulation, we use a linearly polarized laser pulse with a \sin^2 -type temporal envelope

$$E(t) = E_0 \sin^2\left(\frac{\omega t}{2N}\right) \sin(\omega t), \quad (4)$$

where N is the number of optical cycles, E_0 is the peak electric field amplitude, and ω is laser frequency, respectively. For a better fit of the real He atom and He^+ , the value of the softening parameters a and b , respectively, are chosen as 0.5 and 0.3 [28]. The corresponding ionization potentials for the first and second electrons are $I_p^{(1)} = 0.88$ a.u. and $I_p^{(2)} = 2.00$ a.u., respectively. Note that it would be rather time consuming to calculate the total PMD by including all of the ionic channels. In practice, we gradually increase the number of the channels to obtain a convergent PMD. Our calculation shows that the PMD can well converge after considering the lowest four ionic channels.

To more clearly show the electron-correlation effects in the HATI of He, we also simulate the PMD with SAE. The corresponding electron wave function $\vartheta(x, t)$ is obtained by solving the TDSE as follows:

$$i\frac{\partial}{\partial t}\vartheta(x, t) = H_s(x, t)\vartheta(x, t) = \left[\frac{p^2}{2} + V_s(x) + xE(t)\right]\vartheta(x, t), \quad (5)$$

where $V_s(x) = -\frac{1}{\sqrt{x^2+c}}$ and the value of the softening parameter c is chosen as 0.515 to match the ionization potential for the first electron of helium. Similarly, the PMD with SAE is calculated with the part of the wave packet far away from the core by using the Fourier transform method.

B. Wigner distribution functions

The Wigner distribution is interpreted as a quasi-probability distribution in the phase space and is suited to explore the quantum-classical correspondence [29–36]. In this work, we will employ the Wigner distribution to describe the dynamics of the ionized electron during the strong-field single ionization process. For each j th ionic state of He^+ , the corresponding Wigner distribution of the ionized electron in the (x_1, p_1) phase space takes the form [29]

$$W_j(x_1, p_1, t) = \frac{1}{\pi} \int_{-\infty}^{\infty} d\varepsilon \psi_j^*(x_1 + \varepsilon, t) \times \psi_j(x_1 - \varepsilon, t) \exp(2ip_1\varepsilon), \quad (6)$$

where ψ_j is the wave packet of the first electron. Because we study the Wigner distribution of the ionized electron, the ionization part of the wave packet ψ_j is extracted for the calculation [32]. According to Eq. (6), the Wigner distributions for the different ionic channels can be obtained. In practice, for the laser parameters used in our work, the ionization amplitude related to the ionic ground-state channel is dominant, and thus for simplicity we will just study the Wigner distribution of the ionized electron related to the ionic ground-state channel. By tracking the maximal probability density in the Wigner distribution [31–33], one can understand the dynamics of the ionized electron and the electron correlation effect during the strong-field ionization. Note that, different from the classical phase-space probability density function, the value of the Wigner function can be negative, which is due to the quantum nature of the electron wave function [34–36].

III. RESULTS AND DISCUSSIONS

Figure 1 presents the TDSE simulations of the PMDs of He in a few-cycle laser field [$N = 5$ in Eq. (4)] with different wavelengths and intensities. To more clearly show the electron-correlation effect, we also show the SAE results. For the wavelength of 600 nm in Fig. 1(a), the photoelectron yields of He seem qualitatively the same as that calculated with SAE in the low-energy region [$p_1 < 2\sqrt{U_p}$; $U_p = (E_0/2/\omega)^2$], but have a significant enhancement in the high-energy plateau region from HATI ($2\sqrt{U_p} < p_1 < 2\sqrt{5U_p}$). With the increase of laser wavelength from 600 nm

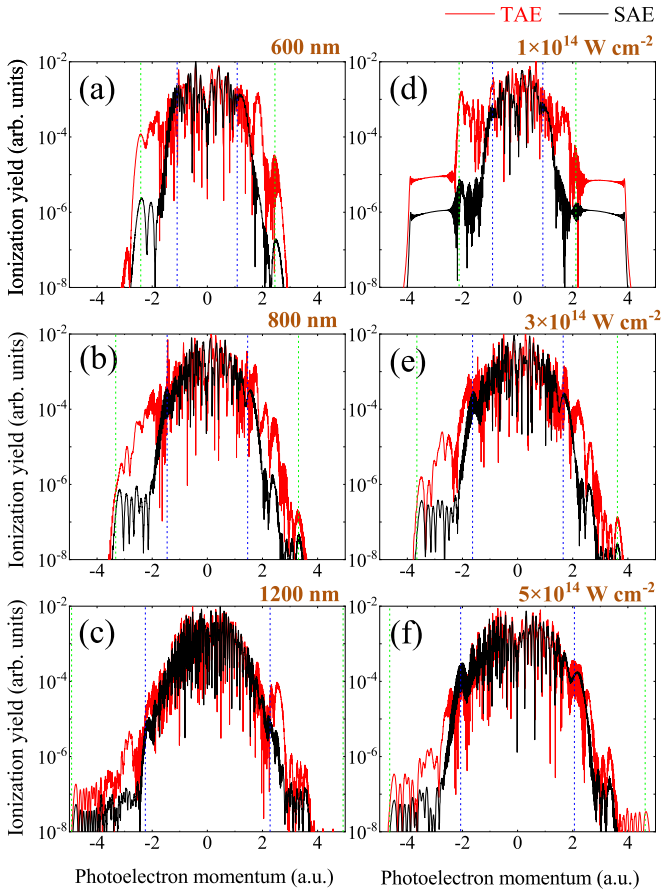


FIG. 1. TDSE-simulated PMDs of a helium atom subject to an intense laser pulse with different laser parameters (red line). For comparison, the SAE results are also presented (black line). (a)–(c) The intensity of the laser field is fixed at $2.5 \times 10^{14} \text{ W cm}^{-2}$ and the wavelengths are 600, 800, and 1200 nm, respectively. (d)–(f) The wavelength is fixed at 800 nm and the laser intensities are 1.0×10^{14} , 3.0×10^{14} , and $5.0 \times 10^{14} \text{ W cm}^{-2}$, respectively. The blue and green dotted lines denote the positions of the $2\sqrt{U_p}$ and $2\sqrt{5U_p}$ cutoffs, respectively.

to 1200 nm, as shown in Figs. 1(a) to 1(c), the HATI enhancement gradually becomes weak. Our result is well consistent with that found in Ref. [20]. On the other hand, we also present the PMDs at different laser intensities in Figs. 1(d) to 1(f). For a low laser intensity in Fig. 1(d), significant enhancement of the HATI amplitude can be also observed in the PAD of He. With the increase of laser intensity, the ionization enhancement in the high-energy plateau region becomes smaller. Therefore, our TDSE simulation clearly shows that, due to the electron correlation effect, the HATI amplitude exhibits a significant enhancement, and moreover, such an enhancement becomes weak for the long laser wavelength or the high laser intensity. In the following, we aim to understand the electron correlation effect on the HATI amplitude and the dependence of the HATI enhancement on the laser parameters, respectively.

To reveal the underlying physics of the electron-correlation effect on the HATI amplitude, a Wigner analysis method is used to show the evolution of the ionized electron wave packet in the phase space. For a laser field with multiple optical

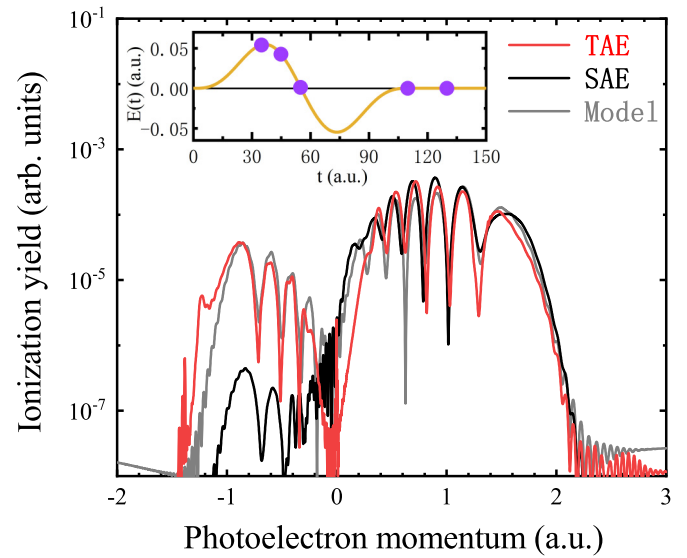


FIG. 2. TDSE-simulated PMD for a single-cycle pulse with the wavelength of 800 nm and the peak intensity of $2.5 \times 10^{14} \text{ W cm}^{-2}$ (red line). For comparison, the SAE result is also presented (black line). TDSE-simulated PMD with the improved SAE model is also shown (gray line). Inset: The electric field of the single-cycle pulse. The violet solid circles in the inset denote the times at which the snapshots of the Wigner distributions will be present.

cycles, the ionized electron wave packet may be emitted at different optical cycles in the laser pulse, which makes the Wigner distribution of the ionized electron too complicated to be well analyzed. To facilitate the understanding of the electronic correlation effect, we thus choose a single-cycle pulse [$N = 1$ in Eq. (4)] with the wavelength of 800 nm and the peak intensity of $2.5 \times 10^{14} \text{ W cm}^{-2}$. The corresponding PMD of He is shown in Fig. 2; see the red line. Similarly, the SAE result is also presented; see the black line. According to the three-step model [4,5], for the laser field we used, the photoelectron with the momentum of $p_1 < 0$ originates from the back-scattered electron that contributes to HATI. Our result clearly shows that the HATI amplitude of He is much larger than that calculated with the SAE, in good agreement with the simulation result shown in Fig. 1.

Figures 3(a) to 3(e) present the snapshots of the Wigner distributions of the ionized electron wave packet of He with TAE at a sequence of times, e.g., $t = 35, 45, 55, 110,$ and 130 a.u., respectively, which are indicated by violet solid circles in the inset of Fig. 2. By tracking the maximal probability density in the Wigner distribution, one can easily understand the dynamics of the ionized electron in the laser field. For example, Fig. 3(a) shows that the ionized electron wave packet is firstly driven away from the parent core along the negative direction of the x_1 axis, which corresponds to the tunneling ionization of an atom in the laser field [37]. Later on, the ionized wave packet continues moving along the negative direction of the x_1 axis in Figs. 3(b) and 3(c). Furthermore, when the laser field reverses its direction, Fig. 3(d) shows that the electron wave packet returns to the core and is strongly forward-scattered (see the trend of distribution over time denoted by the green arrow). In addition, the atom may be

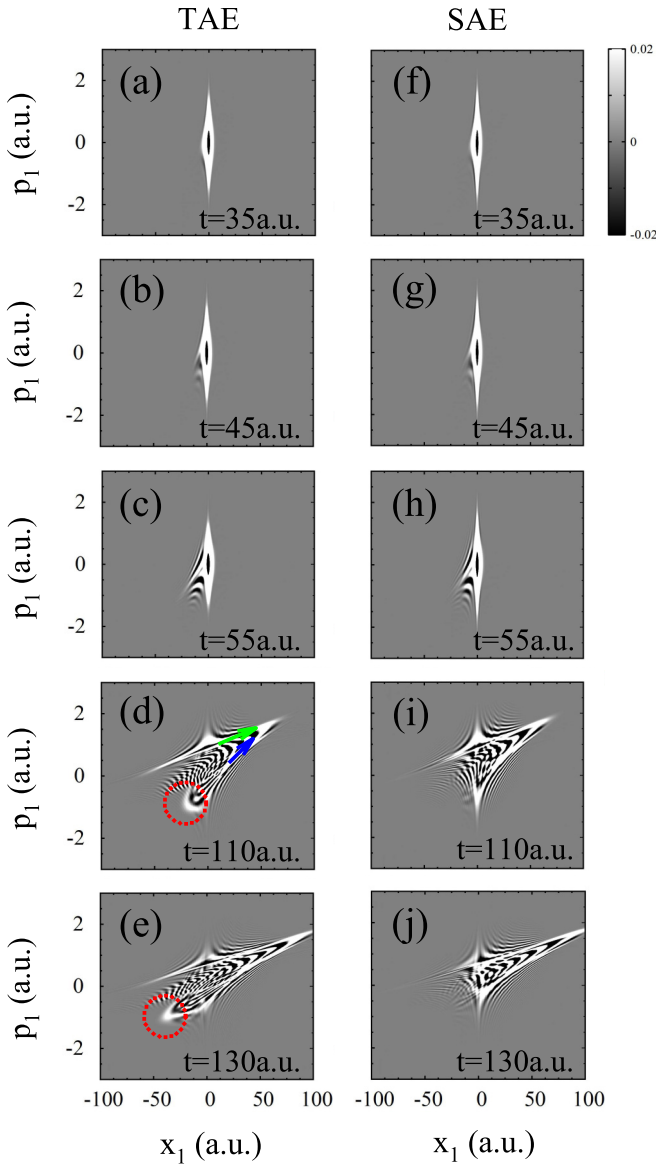


FIG. 3. The snapshots of the Wigner distributions of the ionized electron wave packet at five different times, e.g., $t = 35, 45, 55, 110,$ and 130 a.u., which are indicated by violet solid circles in the inset of Fig. 2. (a)–(e) Helium with TAE and (f)–(j) atom with SAE. The two arrows in (d) denote the trend of distributions in the phase space over time for the forward-rescattered wave packet (green arrow) and the tunneling ionized wave packet (blue arrow). The red dashed circles in (d) and (e) represent the positions of the distribution for the backscattered electron wave packet.

also ionized by tunneling at this time and the corresponding electron wave packet moves along the positive direction of the x_1 axis (see the trend of distribution over time denoted by the blue arrow). After the laser pulse ends ($t > 110$ a.u.), Fig. 3(e) shows that the two kinds of electron wave packets keep moving along the positive direction of the x_1 axis.

To identify the electron correlation effect in the Wigner distributions, we also present the corresponding Wigner distributions of the ionized electron wave packets calculated with SAE in the right column of Fig. 3. As one can see, the Wigner distributions from the TAE and SAE seem almost the same

at $t = 35, 45,$ and 55 a.u., indicating that the influence of the electron correlation on the tunneling ionization is insignificant. On the other hand, for the time $t = 110$ and 130 a.u., the Wigner distributions of the forward-rescattered wave packet and the tunneling ionization wave packet are still almost the same for the TAE and SAE. Thus, for the photoelectron with the momentum of $p_1 > 0$, the PMDs for the TAE and SAE are qualitatively the same, which is well consistent with our simulation shown in Fig. 2. However, a closer inspection reveals that, in comparison with the result from SAE, the Wigner distribution from TAE has an additional distribution near the central core with the momentum of $p_1 < 0$ at $t = 110$ a.u. [see the red dashed circle in Fig. 3(d)], and furthermore, as the time evolves from, e.g., $t = 110$ to 130 a.u., this distribution moves away from the parent core along the negative direction of the x_1 axis [see the red dashed circle in Fig. 3(e)]. Such peculiar Wigner distribution corresponds to the back-scattered electron wave packet, resulting in the enhancement of the HATI amplitude with the momentum of $p_1 < 0$, just as shown in Fig. 2. Such enhancement caused by the electron correlation might be ascribed to a strong Coulomb exclusion effect between the rescattered electron and the remaining electron, which leads to an increase of the backscattering cross section of the return electron.

To confirm our conjecture, we simulate the PMD of He with an improved SAE model, in which the effect of the remaining electron is described with an effective potential

$$H_{e-e}(x) = \frac{1}{\sqrt{(x - x_c)^2 + s}}, \quad (7)$$

where x_c denotes the position of the remaining electron. Due to the Coulomb exclusion between the two electrons during the rescattering, the position of the remaining electron will slightly deviate from the central core. In our simulation, the position offset x_c is chosen as 0.6 a.u., and for a better fit of the $I_p^{(1)}$ of He, the softening parameter s is set as 0.259 . The TDSE-simulated PMD with the improved SAE model is shown by the gray line in Fig. 2, which is qualitatively in a good agreement with the TAE result. Therefore, our result clearly shows that the enhancement of the HATI amplitude is ascribed to the Coulomb exclusion effect between the remaining electron and the rescattered electron during the rescattering.

Finally, we discuss the dependence of the HATI enhancement caused by the Coulomb exclusion effect on the laser parameters. Just as shown in Fig. 1, the increase of laser wavelength and intensity leads to better agreement between the simulations of TAE and SAE. A possible reason is that, with increasing laser wavelength or intensity, the return energy of the electron will increase accordingly [4,5], and hence, the Coulomb exclusion effect of the remaining electron on the return electron becomes relatively weak. To more intuitively show the dependence of the Coulomb exclusion effect on the laser parameters, we simulate the scattering of a free electronic wave packet by a cation He^+ in terms of Wigner distributions. To facilitate the analysis, the initial wave function of the recolliding electron is described with a Gaussian function $\psi_0(x_1) = (2\pi\sigma)^{-1/4} \exp[-(x_1 - x_0)^2/\sigma + iv_0(x_1 - x_0)]$ with an initial velocity of v_0 and position of x_0 , and the cation

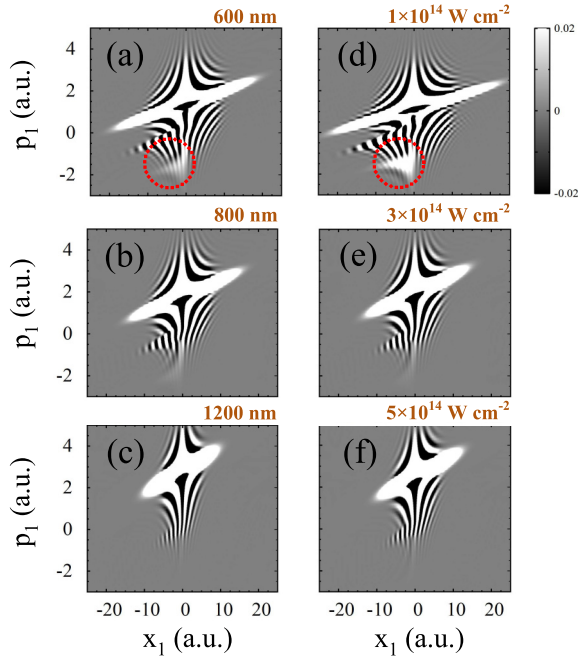


FIG. 4. The snapshots of the Wigner distributions for the scattering of a free electronic wave packet by a cation He^+ . The corresponding electron velocity is calculated with the laser parameters used in Fig. 1. For more details, see the text.

He^+ is initially in the ground state. In our simulation, the velocity of the electron is given according to the maximal return energy of the rescattered electron in the laser field $v_0 \sim \sqrt{2 \times 3.17 U_p}$, the initial position is set as, e.g., $x_0 = 20$ a.u. and $\sigma = 2$. Figure 4 presents the snapshots of the Wigner distribution at the time when the electronic wave packet reaches the central core and the corresponding electron velocity is calculated with the laser parameters used in Fig. 1. For short wavelengths or low intensities of the laser fields in Figs. 4(a) and 4(d), the velocity of the free electron is small and accordingly the pronounced distributions for the back-scattered wave packet caused by the Coulomb exclusion effect can be well observed (see the red dashed circles). However, with increasing wavelength or intensity of the laser field, the elec-

tron velocity increases and the corresponding distribution for the back-scattered wave packet gradually disappears. The change of the back-scattered wave packet amplitude with the laser parameters is well consistent with the simulation shown in Fig. 1. Therefore, our result clearly shows that the dependence of the HATI enhancement for He atom on the laser parameters is ascribed to the Coulomb exclusion effect with respect to the return energy of the rescattered electron.

IV. CONCLUSION

In summary, we theoretically studied the electron correlation effects on the HATI of a He atom with TAE. We find that the HATI amplitude of a He atom shows a significant enhancement in comparison with the SAE results, and moreover, such enhancement becomes weak for long laser wavelength or high laser intensity. By performing the Wigner analysis, we clearly show that the enhancement is due to a strong Coulomb exclusion effect of the remaining electron on the rescattered electron. With the increase of laser wavelength or intensity, the return energy of the rescattered electron increases and accordingly the Coulomb exclusion effect of the remaining electron decreases. Our work suggests the Wigner distribution in phase space as a feasible tool in analyzing photoionized electron wave packet dynamics and provides a deep understanding of two-electron correlated dynamics in strong field ionization.

ACKNOWLEDGMENTS

We thank Jing Chen and Li Guo for useful discussions. This work is supported by the National Key Program for S&T Research and Development (Grant No. 2019YFA0307702), the National Natural Science Foundation of China (Grants No. 12121004, No. 11922413, No. 11874392, No. 11834015, No. 11804374, No. 11847243, and No. 12004391), the Strategic Priority Research Program of the Chinese Academy of Sciences (Grant No. XDB21010400), the China Postdoctoral Science Foundation (Grants No. 2020T130682 and No. 2019M662752), the Science and Technology Department of Hubei Province (Grant No. 2020CFA029), and the K.C. Wong Education Foundation.

- [1] P. Agostini, F. Fabre, G. Mainfray, G. Petite, and N. K. Rahman, *Phys. Rev. Lett.* **42**, 1127 (1979).
- [2] G. G. Paulus, W. Nicklich, H. Xu, P. Lambropoulos, and H. Walther, *Phys. Rev. Lett.* **72**, 2851 (1994).
- [3] A. Lohr, M. Kleber, R. Kopold, and W. Becker, *Phys. Rev. A* **55**, R4003 (1997).
- [4] P. B. Corkum, *Phys. Rev. Lett.* **71**, 1994 (1993).
- [5] K. J. Schafer, B. Yang, L. F. DiMauro, and K. C. Kulander, *Phys. Rev. Lett.* **70**, 1599 (1993).
- [6] X. Xie, S. Roither, D. Kartashov, E. Persson, D. G. Arbó, L. Zhang, S. Grafe, M. S. Schöffler, J. Burgdörfer, A. Baltuška, and M. Kitzler, *Phys. Rev. Lett.* **108**, 193004 (2012).
- [7] M. Meckel *et al.*, *Science* **320**, 1478 (2008).
- [8] G. G. Paulus, F. Grasbon, H. Walther, P. Villorosi, M. Nisoli, S. Stagira, E. Priori, and S. De Silvestri, *Nature (London)* **414**, 182 (2001).
- [9] D. B. Milošević, G. G. Paulus, and W. Becker, *Phys. Rev. Lett.* **89**, 153001 (2002).
- [10] C. I. Blaga, J. Xu, A. D. Dichiaro, E. Sistrunk, K. Zhang, P. Agostini, T. A. Miller, L. F. Dimauro, and C. D. Lin, *Nature (London)* **483**, 194 (2012).
- [11] J. Xu, C. I. Blaga, K. Zhang, Y. Lai, C. D. Lin, T. A. Miller, P. Agostini, and L. F. Dimauro, *Nat. Commun.* **5**, 4635 (2014).
- [12] R. P. Sun, X. Y. Lai, S. G. Yu, Y. L. Wang, S. P. Xu, W. Quan, and X. J. Liu, *Phys. Rev. Lett.* **122**, 193202 (2019).
- [13] C. A. Nicolaides, S. Dionissopoulou, and T. Mercouris, *J. Phys. B* **31**, L1 (1998).
- [14] A. D. Bandrauk and H. Z. Lu, *Phys. Rev. A* **72**, 023408 (2005).
- [15] H. Akagi, T. Otobe, A. Staudte, A. Shiner, F. Turner, R. Döner, D. M. Villeneuve, and P. B. Corkum, *Science* **325**, 1364 (2009).
- [16] B. Zhang, J. Yuan, and Z. Zhao, *Phys. Rev. Lett.* **111**, 163001 (2013).

- [17] Z. Zhao and J. Yuan, *Phys. Rev. A* **89**, 023404 (2014).
- [18] J. Rapp and D. Bauer, *Phys. Rev. A* **89**, 033401 (2014).
- [19] Y. L. Wang, S. G. Yu, X. Y. Lai, X. J. Liu, and J. Chen, *Phys. Rev. A* **95**, 063406 (2017).
- [20] C. Yu and L. B. Madsen, *Phys. Rev. A* **95**, 063407 (2017).
- [21] R. Grobe and J. H. Eberly, *Phys. Rev. Lett.* **68**, 2905 (1992).
- [22] D. Bauer, *Phys. Rev. A* **56**, 3028 (1997).
- [23] M. W. Shi, X. Y. Lai, and X. J. Liu, *J. Phys. B* **54**, 115601 (2021).
- [24] L. Lehtovaara, J. Toivanen, and J. Eloranta, *J. Comput. Phys.* **221**, 148 (2007).
- [25] M. D. Feit, J. A. Fleck, Jr., and A. Steiger, *J. Comput. Phys.* **47**, 412 (1982).
- [26] M. R. Hermann and J. A. Fleck, Jr., *Phys. Rev. A* **38**, 6000 (1988).
- [27] W. Y. Wu and F. He, *Sci. Rep.* **8**, 14933 (2018).
- [28] P. C. Li, X. X. Zhou, G. L. Wang, and Z. X. Zhao, *Phys. Rev. A* **80**, 053825 (2009).
- [29] E. Wigner, *Phys. Rev.* **40**, 749 (1932).
- [30] F. He, A. Becker, and U. Thumm, *Phys. Rev. Lett.* **101**, 213002 (2008).
- [31] M. Lein, E. K. U. Gross, and V. Engel, *Phys. Rev. Lett.* **85**, 4707 (2000).
- [32] S. Gräfe, J. Doose, and J. Burgdörfer, *J. Phys. B* **45**, 055002 (2012).
- [33] H. J. Kull, *New. J. Phys.* **14**, 055013 (2012).
- [34] A. Czirják, R. Kopold, W. Becker, M. Kleber, and W. P. Schleich, *Opt. Commun.* **179**, 29 (2000).
- [35] N. Teeny, E. Yakaboylu, H. Bauke, and C. H. Keitel, *Phys. Rev. Lett.* **116**, 063003 (2016).
- [36] M. Han, P. Ge, Y. Fang, X. Yu, Z. Guo, X. Ma, Y. Deng, Q. Gong, and Y. Liu, *Phys. Rev. Lett.* **123**, 073201 (2019).
- [37] W. Becker, F. Grasbon, R. Kopold, D. B. Milošević, G. G. Paulus, and H. Walther, *Adv. At. Mol. Opt. Phys.* **48**, 35 (2002).